Cement & Concrete Composites 33 (2011) 171–178

Contents lists available at ScienceDirect

Cement & Concrete Composites

journal homepage: www.elsevier.com/locate/cemconcomp

Viscoelastic properties and drying stress extracted from concrete ring tests

Zachary C. Grasley [a,*], Matthew D. D'Ambrosia [b]

[a] 503C CE/TTI Bldg., 3136 TAMU, College Station, TX 77845, USA
[b] CTL Group, 5400 Old Orchard Rd., Skokie, IL 60077, USA

ARTICLE INFO

Article history:
Received 8 June 2010
Received in revised form 15 October 2010
Accepted 20 October 2010
Available online 26 October 2010

Keywords:
Ring test
Shrinkage
Solidification
Viscoelastic

ABSTRACT

Passive restrained concrete ring experiments provide enough information to extract useful aging viscoelastic constitutive properties when combined with free drying shrinkage and mass loss experiments. In this paper, analytical techniques are described for deriving a closed-form solution to extract the viscoelastic Young's modulus from solidifying concrete in a restrained concrete ring test. Using limit theorems, approximate closed-form solutions are derived for the non-uniform internal relative humidity (*RH*), free drying shrinkage, and tangential stress gradients. An example problem demonstrates the utility of the derived solutions and illustrates the effect that viscoelastic relaxation and solidification have on the tangential stress profile in the restrained, drying concrete ring. Both viscoelastic and solidification effects have a significant impact on the predicted stress profile.

1. Introduction

Passive restraint tests have become increasingly popular as experimental methods for quantifying the sensitivity of certain concrete mixtures to cracking due to restrained free strains. Free strains, while typically drying shrinkage or thermal strains, can be any environmentally induced strain (not induced by external loading). To date, passive restraint tests have been utilized primarily in a qualitative fashion such that information regarding the aging viscoelastic properties of the solidifying concrete is not directly determined from the tests. While the time to cracking in restrained concrete specimens is a beneficial parameter for screening concrete mixtures, passive restraint tests are also capable of yielding fundamental constitutive behavior of early-age, solidifying concrete.

Current passive restraint tests for concrete can be subdivided into two basic geometrical categories: uniaxial tests and ring tests. This paper will focus on the ring test [1–8]; solutions for extracting the viscoelastic Young's modulus from axial restraint tests may be found elsewhere [9]. Ring tests consist of a thick concrete ring surrounding a thinner steel (or other metal) restraining ring. As concrete shrinks, the inner ring partially restrains the movement, and stress develops. If the degree of restraint is large enough (i.e. the thickness and stiffness of the inner ring high enough), the concrete will crack and stored strain energy will be released. A typical ring test is illustrated in Fig. 1. The strain on the inner surface of the restraining ring is often measured; not only can this strain be used to calculate the stress distribution in the concrete as suggested by Weiss et al. [2–5], but it can also be used to determine the aging viscoelastic Young's modulus of the shrinking concrete.

The restrained ring shrinkage test was first developed for use in testing concrete during the 1930s [10]. It was envisioned as a comparative test technique to evaluate the potential for concrete drying shrinkage cracking in buildings. Early versions of the test apparatus were not instrumented with strain gages and therefore did not provide quantitative feedback regarding the magnitude of stress or strain development. The only quantitative result obtained from early ring tests was concrete cracking time, obtained from daily visual observation of the concrete surface.

It was during the late 1980s and early 1990s that a resurgence of interest in the ring test occurred in order to study the early age cracking issues observed in high performance or high strength concrete [11–15]. A new version of the test apparatus evolved, which consisted of an instrumented inner steel restraining ring to quantitatively evaluate stress development. An advantage of the instrumented ring, which consists of resistance-based strain gages mounted along the inner surface of the restraining ring, was that the cracking time could be determined with more precision by observing the measured drop in restraining ring strain. This revised version of the ring test led to the development of two standard test methods, the AASHTO provisional standard PP-34 and ASTM C1581. There are slight geometrical differences between the two standard tests, with the AASHTO version having a thicker concrete cross section and thus taking longer to crack. The ASTM version, first published in 2004, only has a 38 mm cross sectional thickness, so it is recommended to limit the aggregates to 12.5 mm maximum. The ring test has been used for the evaluation of many

* Corresponding author. Tel.: +1 979 845 9961; fax: +1 979 458 0780.
E-mail address: zgrasley@civil.tamu.edu (Z.C. Grasley).

0958-9465/$ - see front matter © 2010 Elsevier Ltd. All rights reserved.
doi:10.1016/j.cemconcomp.2010.10.014

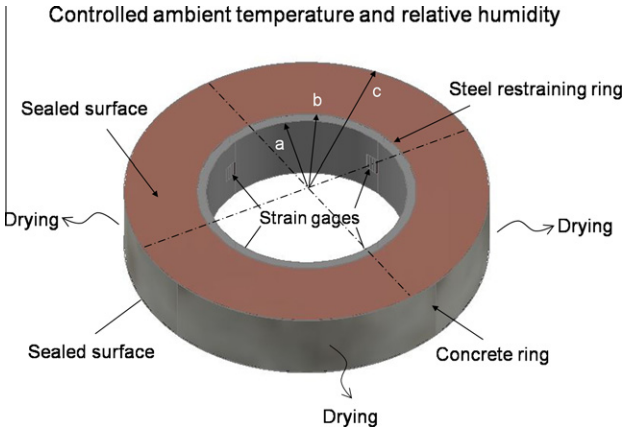

Fig. 1. Typical restrained concrete ring test configuration. Concrete shrinks while radially drying, compressing the inner steel ring. Strain is measured at the inner surface of the restraining ring as a function of time. Typical dimensions are $a \approx 14$ cm, $b \approx 15$ cm, and $c \approx 25$ cm.

concrete types, from high performance and high strength concretes [16], concrete containing silica fume [12] or shrinkage reducing admixtures [17], fiber reinforced concrete [13], self consolidating concrete [18], and concrete repair materials [18].

The objective of this paper is to derive closed-form analytical solutions for determining the solidifying, viscoelastic Young's modulus of concrete using data obtained from the restrained concrete ring test. Additionally, approximate analytical solutions for non-uniform stress gradients of radially drying concrete rings will be derived as a function of the measured mass loss and spatially averaged free strain measured with companion concrete prisms.

By extracting fundamental material properties from simple passive restraint tests, the utility of such tests increases substantially. Viscoelastic material properties obtained from the restrained concrete ring test could be implemented in structural models to predict real stress distributions in concrete infrastructure, improving prediction of damage in such structures and providing a means for evaluating preventive measures such as extended wet curing. In the remaining sections of this paper, a form of the solidifying viscoelastic constitutive equation allowing analytical solution of the ring test will be introduced, and the solutions derived for both the viscoelastic Young's modulus and non-uniform stress gradients in radially drying concrete.

2. Constitutive model

While Grasley and Lange [19] have shown that the viscoelastic aging of cement pastes at early ages cannot be fully accounted for by the solidification theory, solidification is still the primary source of aging during this period. Thus, the constitutive equation for early age concrete can be approximated by the solidification theory. According to the solidification theory [20,21], the constitutive equation of a solidifying viscoelastic material may be expressed according to:

$$\dot{\varepsilon}(t) = \frac{E^0 \dot{\sigma}(t)}{v(t)} + \frac{1}{v(t)} \int_0^t J^g(t-t')\dot{\sigma}(t')dt' + \dot{\varepsilon}^f(t), \tag{1}$$

where t is elapsed time, $\varepsilon(t)$ is the time dependent uniaxial strain, E^0 is the elastic Young's modulus at an age where $v(t) = 1$, $\sigma(t)$ is the uniaxial stress, $v(t)$ is the aging function that represents the degree of solidification, $J^g(t)$ is the viscoelastic uniaxial compliance of the non-aging solid (that is solidifying), $\varepsilon^f(t)$ is the free strain, and the overhead dots denote the partial derivative with respect to time.

The presence of the time derivatives and integral preclude the direct implementation of Eq. (1) in elastic solutions for the restrained ring tests. A typical method of accounting for the time history dependence of viscoelastic materials in such a way as to allow use of existing elastic solutions is to utilize the elastic–viscoelastic correspondence principle [22]. The correspondence principle involves utilizing Laplace or Fourier transforms to eliminate differential operators, transforming the viscoelastic constitutive equation into the same algebraic form as for elastic materials. This transformation allows the direct use of elastic solutions for solving the transformed viscoelastic problem. Upon obtaining the solution in the transform domain, inversion yields the solution in the time domain. Unfortunately, the constitutive equation for solidifying materials does not allow use of the classic correspondence principle since it involves the product of a time-dependent function and a convolution integral, resulting in a convolution in the transform domain. In order to utilize the correspondence principle for solidifying materials, Grasley and Lange [19] modified the classic correspondence principle, solving for the transformed strain as

$$\bar{\varepsilon}(s) = \sum_{i=1}^{n} \beta_i \frac{(s+\omega_i)^2}{s} \bar{J}^g(s)\bar{\sigma}(s+\omega_i) + \bar{\varepsilon}^f(s). \tag{2}$$

The overbars denote the Laplace transformed parameter with the transform parameter s, and the aging function is expressed as

$$\frac{1}{v(t)} = \sum_{i=1}^{n} \beta_i e^{-\omega_i t}, \tag{3}$$

where β_i and ω_i are fit parameters. Eq. (2) is in the same algebraic form as the elastic constitutive equation, allowing one to utilize elastic solutions where the elastic strain is substituted by $\bar{\varepsilon}(s)$, the elastic uniaxial compliance replaced by $\bar{J}^g(s)$, the stress replaced by $(s+\omega_i)^2\bar{\sigma}(s+\omega_i)\beta_i/s$, and the free strain replaced by $\bar{\varepsilon}^f(s)$.

Likewise, a modified correspondence principle (see Appendix A) may be used to solve the viscoelastic problem for a solidifying material with the constitutive equation written in terms of the strain history. If the aging function is expressed as

$$v(t) = \kappa(1 - \exp(-\lambda t)), \tag{4}$$

where κ and λ are fit parameters, one can write the transformed constitutive equation according to:

$$\bar{\sigma}(s) = \kappa\bar{E}^g(s)\left\{(s\bar{\varepsilon}(s) - (s+\lambda)\bar{\varepsilon}(s+\lambda)) - (s\bar{\varepsilon}^f(s) - (s+\lambda)\bar{\varepsilon}^f(s+\lambda))\right\}, \tag{5}$$

where $\bar{E}^g(s)$ is the Laplace transformed, non-aging viscoelastic Young's modulus of the solidifying material (solidifying "gel"). As with Eq. (2), Eq. (5) is in the same algebraic form as its elastic equivalent. In the application of Eq. (5) with elastic solutions to solve for the transformed viscoelastic stress, the elastic Young's modulus is replaced by $\kappa\bar{E}^g(s)$, the elastic strain is replaced by $(s\bar{\varepsilon}(s) - (s+\lambda)\bar{\varepsilon}(s+\lambda))$, and the free strain is replaced by $(s\bar{\varepsilon}^f(s) - (s+\lambda)\bar{\varepsilon}^f(s+\lambda))$.

Since the solidification function has an equivalent effect on both viscoelastic and elastic moduli, the simplest way to obtain the aging function is to fit measured elastic moduli as a function of age, normalizing the function to unity at the age where E^0 is specified. If the age of initial applied displacement does not occur at $t = 0$, then (4) may be shifted such that $t = 0$ coincides with the initial displacement age. Shifting (4) may be accomplished according to:

$$v(t) = \kappa(1 - \exp(-\lambda(t+t'))), \tag{6}$$

where t' is the age at initial applied displacement; with this modification, (5) becomes

$$\bar{\sigma}(s) = \kappa\bar{E}^g(s)\left\{\left(s\bar{\varepsilon}(s) - (s+\lambda)\bar{\varepsilon}(s+\lambda)/e^{\lambda t'}\right) - \left(s\bar{\varepsilon}^f(s) - (s+\lambda)\bar{\varepsilon}^f(s+\lambda)/e^{\lambda t'}\right)\right\}, \tag{7}$$

such that the elastic strain is now replaced by $(s\bar{\varepsilon}(s)-(s+\lambda)\bar{\varepsilon}(s+\lambda)/e^{\lambda t'})$ and the free strain is replaced by $(s\bar{\varepsilon}^f(s)-(s+\lambda)\bar{\varepsilon}^f(s+\lambda)/e^{\lambda t'})$. Inversion of (7) into the time domain yields $\sigma(t)$, where $t = 0$ corresponds to the time of initial application of displacement. Therefore, the actual age of a specimen at any time t is $t + t'$.

3. Solution to the ring test with radially variable free strain

See et al. [7] devised solutions to determine the stress in the outer concrete ring from the measured tangential strain on the inside of the restraining ring based on the assumption of thin cross-section, while Weiss et al. extended the solution for a thick walled concrete ring under uniform [1,2] or radially varying free strain conditions [4]. Hossain and Weiss [2] solved the ring test geometry for a time-dependent "effective elastic modulus" (which approximates the viscoelastic modulus) in terms of the measured tangential strain of the inner restraining ring. The following derivation will solve the ring geometry for a solidifying viscoelastic material considering a radially and time dependent free strain. The elastic solution will be expressed first such that the modified correspondence principle derived in this paper can be implemented.

The small displacement gradient elastic solution for the ring test involves utilizing Lame's plane stress solution for both the inner and outer rings, then using equilibrium conditions at the interface to solve for the interfacial pressure. The tangential and radial stresses in the inner, restraining ring are (respectively)

$$\sigma_\theta^s(r,t)=\frac{E^sC_1}{1-\nu^s}+\frac{E^sC_2}{(1+\nu^s)r^2}, \tag{8}$$

and

$$\sigma_r^s(r,t)=\frac{E^sC_1}{1-\nu^s}-\frac{E^sC_2}{(1+\nu^s)r^2}, \tag{9}$$

where E^s is the Young's modulus of the inner ring, ν^s is the Poisson's ratio of the inner ring, r is the radial coordinate, and C_1 and C_2 are constants. The boundary conditions are

$$\begin{aligned}&\sigma_r^s(a,t)=0,\\&\sigma_r^s(b,t)=P(t),\end{aligned} \tag{10}$$

where a is the inner radius of the inner ring, b is the outer radius of the inner ring, and P is the pressure applied on the inner ring by the outer concrete ring. From (8)–(10), C_1 and C_2 may be determined such that the stresses in the inner ring are

$$\sigma_\theta^s(r,t)=\frac{b^2P(t)(a^2+r^2)}{(b^2-a^2)r^2} \tag{11}$$

and

$$\sigma_r^s(r,t)=\frac{b^2P(t)(a^2-r^2)}{(a^2-b^2)r^2}. \tag{12}$$

The plane stress elastic constitutive equation for the inner ring is

$$\varepsilon_\theta^s(r,t)=\frac{\sigma_\theta^s(r,t)-\nu^s\sigma_r^s(r,t)}{E^s}, \tag{13}$$

such that

$$\varepsilon_\theta^s(r,t)=\frac{b^2P(t)\{a^2(1+\nu^s)-r^2(\nu^s-1)\}}{(b^2-a^2)E^sr^2}. \tag{14}$$

The stresses in the elastic, outer concrete ring can be expressed as [23]

$$\sigma_\theta^c(r,t)=\frac{E^c}{r^2}\int_b^r r'\varepsilon^f(r',t)dr'-E^c\varepsilon^f(r,t)+\frac{E^cC_3}{1-\nu_c}+\frac{E^cC_4}{(1+\nu^c)r^2}, \tag{15}$$

and

$$\sigma_r^c(r,t)=\frac{-E^c}{r^2}\int_b^r r'\varepsilon^f(r',t)dr'+\frac{E^cC_3}{1-\nu^c}-\frac{E^cC_4}{(1+\nu^c)r^2}, \tag{16}$$

where $\varepsilon^f(r,t)$ is the free strain, E^c and ν^c are, respectively, the Young's modulus and Poisson's ratio of the outer concrete ring, and C_3 and C_4 are constants. The boundary conditions for the outer ring are

$$\begin{aligned}&\sigma_r^c(b,t)=P(t)\\&\sigma_r^c(c,t)=0.\end{aligned} \tag{17}$$

By combining (15)–(17) and (14) (solved for $P(t)$), the stresses in the outer ring can be determined as a function of the tangential strain at the inner radius of the inner ring ($\varepsilon_a(t)=\varepsilon_\theta^s(a,t)$) as

$$\sigma_\theta^c(r,t)=\frac{(b-a)(a+b)E^s(c^2+r^2)\varepsilon_a(t)}{2(b-c)(b+c)r^2}-\frac{2E^c\left((b^2+r^2)\int_b^c r'\varepsilon^f(r',t)dr'-(b-c)(b+c)(\int_b^r r'\varepsilon^f(r',t)dr'-r^2\varepsilon^f(r,t))\right)}{2(b-c)(b+c)r^2} \tag{18}$$

and

$$\sigma_r^c(r,t)=\frac{(a^2-b^2)E^s(c^2-r^2)\varepsilon_a+2E^c\left((b^2-r^2)\int_b^c r'\varepsilon^f(r',t)dr'+(c^2-b^2)\int_b^r r'\varepsilon^f(r',t)dr'\right)}{2(b^2-c^2)r^2}. \tag{19}$$

The plane stress constitutive equation for the tangential strain of the outer concrete ring is

$$\varepsilon_\theta^c(r,t)=\frac{\sigma_\theta^c(r,t)-\nu^c\sigma_r^c(r,t)}{E^c}+\varepsilon^f(r,t). \tag{20}$$

For cylindrical coordinates with tangential symmetry (i.e. the strain does not vary as a function of θ), the strain–displacement relation for the tangential strain is

$$u_r(r,t)=\frac{\varepsilon_\theta(r,t)}{r}. \tag{21}$$

Using (18)–(21), the displacement $u_r(b,t)$ can be determined for both the inner and outer rings. For displacement continuity, the displacements at the interface may be equated. Furthermore, the Young's modulus of the outer concrete ring may be solved for as

$$E^c=\frac{(a-b)(a+b)E^s\varepsilon_a(t)(b^2(\nu^c-1)-c^2(\nu^c+1))}{4b^2\underline{\varepsilon}^f(t)+(b-c)(b+c)\varepsilon_a(t)\left\{(a^2(\nu^s+1)-b^2(\nu^s-1))\right\}}. \tag{22}$$

where $\underline{\varepsilon}^f(t)=\int_b^c r'\varepsilon^f(r',t)dr'$. Using the correspondence principle outlined in a previous section of this paper, the viscoelastic Young's modulus of the non-aging, solidifying gel may be determined according to:

$$\bar{E}^g(s)=\frac{1}{\kappa}\times\frac{(a-b)(a+b)\frac{E^s}{s}D_1(s)(s)(b^2(\nu^c-1)-c^2(\nu^c+1))}{4b^2(s\bar{\underline{\varepsilon}}^f(s)-(s+\lambda)\bar{\underline{\varepsilon}}^f(s+\lambda))+(b-c)(b+c)D_1(s)\{(a^2(\nu^s+1)-b^2(\nu^s-1))\}}, \tag{23}$$

where

$$D_1(s)=s\bar{\varepsilon}_a(s)-\frac{(s+\lambda)}{e^{\lambda t'}}\bar{\varepsilon}_a(s+\lambda). \tag{24}$$

In (23), the viscoelastic Poisson's ratio of the concrete is assumed to be constant and equal to the elastic value for reasons discussed in [24]. Inversion of (23) into the time domain yields $E^g(t)$ – the non-aging viscoelastic Young's modulus of the solidifying phase of the concrete. The viscoelastic Young's modulus of the bulk concrete at any age may be determined according to:

$$E^c(t,t') = v(t')E^g(t-t'), \tag{25}$$

where $E^g(t-t')$ comes from inverting (23) and $v(t')$ comes from (4). It should be noted that if concrete behaves in a linear fashion and damage does not develop, then E^g calculated from (23) is independent of geometry. The geometry terms are present in (23) because of the effect of geometry embedded in $\overline{\varepsilon}^f$, but the geometry effects cancel each other when concrete behaves linearly and no damage develops. As the ring test geometry changes the peak tensile stress magnitude changes. Therefore, in real concrete, which behaves nonlinearly and does develop damage, the effect of changes in the peak tensile stress magnitude is such that the probability of nonlinear response and damage changes. Therefore, one could conceivably compare the extracted E^g from ring tests or uniaxial tests [9] utilizing different geometries in order to quantify the damage or nonlinearity that develops in restrained, drying concrete.

4. Determination of free strain profile

In order to utilize (23) to determine the viscoelastic Young's modulus of solidifying concrete, it is necessary to quantify the free strain profile in the ring in the transform domain, $\overline{\varepsilon}^f(r,s)$. A common test that accompanies the concrete ring test is the measurement of mass loss (Δm) and spatially averaged free shrinkage ($\langle \varepsilon^f(t) \rangle$) of a symmetrically drying (from two parallel sides) concrete prism. With the measured mass loss and shrinkage data for the prismatic specimen, Grasley [9] has shown that the free shrinkage strain of concrete caused by drying can be approximated in the transform domain by

$$\overline{\varepsilon}^f(r,s) = -1.1\left(\frac{RH_{initial}}{s} - \overline{RH}(r,s)\right)M, \tag{26}$$

where $RH_{initial}$ is the internal relative humidity (RH) in the concrete at the start of drying, $\overline{RH}(r,s)$ is the transformed internal RH distribution in the concrete ring, and M is a term that encompasses the constitutive properties of the concrete. If the desorption isotherm for the concrete is expressible as [25]

$$S(RH) = 1 - 0.75\left(1 - \left(\frac{RH}{100}\right)^3\right), \tag{27}$$

where $0 \le S \le 1$ is the degree of liquid saturation of the pores, then (26) agrees quite well ($R^2 = 0.997$) with the transformed poromechanical expression for shrinkage given in [9] for an RH reduction up to 50%. For desorption isotherms different than (26) the error will be greater, although (26) could easily be modified to be used with alternative expressions for $S(RH)$.

If the symmetrically drying concrete prism is placed in an environment with a constant ambient RH (RH_{bound}) and a temperature of 20 °C, then M may be expressed as [9]

$$M = \frac{0.4L\langle \varepsilon^f(t) \rangle}{\sqrt{D}\sqrt{t}(RH_{initial} - RH_{bound})}, \tag{28}$$

where D is the drying diffusion coefficient, t is elapsed time since the start of drying, and L is the width of the concrete prism in the direction of drying. The drying diffusion coefficient may be directly measured or approximated according to [9]

$$D = \frac{L^2\pi(RH_{initial}^2 - A + B)}{16(RH_{bound} - RH_{initial})^2 t}, \tag{29}$$

where

$$A = \frac{215.726\ RH_{initial}(\Delta m(t) + 0.75\phi V\rho - 1)^{1/3}}{\phi^{1/3}V^{1/3}\rho^{1/3}} \tag{30}$$

and

$$B = \frac{11634.4(\Delta m(t) + 0.75\phi V\rho - 1)^{2/3}}{\phi^{2/3}V^{2/3}\rho^{2/3}}. \tag{31}$$

Here, $\Delta m(t)$ is the mass loss of the prismatic specimen at time t, V is the volume of the prism, ϕ is the pore volume fraction (porosity), and ρ is the density of water. The functions described in (28)–(31) are valid only in the early stages of drying, or until the average internal RH in the concrete prism has decreased to about halfway between $RH_{initial}$ and RH_{bound}. For concrete, this early stages limitation is not an issue of concern since concrete dries slowly and cracks generally form in the restrained ring test before substantial drying has occurred.

The transformed internal RH distribution in the concrete ring, $\overline{RH}(r,s)$, may be approximated according to (B.5) in Appendix B. The combination of (26)–(31) and (B.5) results in a closed-form expression for $\overline{\varepsilon}^f(r,s)$ in the drying concrete ring.

In order to solve (23), not only is $\overline{\varepsilon}^f(r,s)$ needed, but also $\underline{\overline{\varepsilon}}^f(s)$. Using the modified correspondence principle derived in this paper with the expression for $\underline{\varepsilon}^f(t)$ presented earlier, one finds that

$$\underline{\overline{\varepsilon}}^f(s) = -1.1M\left\{\frac{(c^2-b^2)}{2s}RH_{initial} - \underline{\overline{RH}}(c,s)\right\}, \tag{32}$$

where

$$\underline{\overline{RH}}(r,s) = \int_b^r r'\overline{RH}(r,s)dr'. \tag{33}$$

A closed-form, simplified early drying expression for $\underline{\overline{RH}}(r,s)$ is given by (B.8) in Appendix B. Combining (B.8) with (32) results in a closed-form expression for $\underline{\overline{\varepsilon}}^f(s)$. Inserting $\underline{\overline{\varepsilon}}^f(s)$ and $\underline{\overline{\varepsilon}}^f(s+\lambda)$ into (23) along with the geometry of the experiment and properties of the inner ring allows the determination of $\overline{E}^g(s)$. Inversion into the time domain yields $E^g(t)$.

5. Example

5.1. Extraction of viscoelastic Young's modulus

An example calculation will demonstrate the utility of the preceding derivations. Consider a restrained ring test represented by Fig. 1, where a = 14 cm, b = 15 cm, and c = 25 cm. Let $RH_{initial}$ = 100 and RH_{bound} = 50. Considering a plain steel inner restraining ring, E^s = 200 GPa and v^s = 0.3. While an approach is outlined above for determining M and D from measurements of mass loss and free drying shrinkage of a companion concrete prism specimen, for simplicity we will assume that D and M are both constant and given by $D = 1\ \text{cm}^2/\text{d}$ and $M = 8.3 \times 10^{-6}$ 1/MPa, respectively. An example illustrating the calculation of M and D from prism measurements is presented elsewhere [9]. If we set $v^f = 0.2$ and the aging parameters $\kappa = 1.7$ and $\lambda = 0.3$, the aging function representing the rate of solidification is as shown in Fig. 2. Let the age of the concrete at the start of drying be 1 d (i.e. $t' = 1$), and the tangential strain measured on the inner face of the steel be

$$\varepsilon_a(t) = -16.7 \times 10^{-6} t^{0.3}. \tag{34}$$

As mentioned previously, t represents the time from the start of drying such that the actual age of the specimen is $t + t'$ at any time. Combining the Laplace transform of (34) with inputs listed above allows the direct calculation of $\overline{E}^g(s)$. Subsequent inversion into the time domain results in $E^g(t)$, and application of (25) results in the determination of the aging (solidifying) viscoelastic Young's modulus of the concrete as shown in Fig. 3. As expected, the effect of solidification is such that as the age of applied constant displacement increases, the elastic Young's modulus ($E^c(t',t')$) increases and the relaxation decreases.

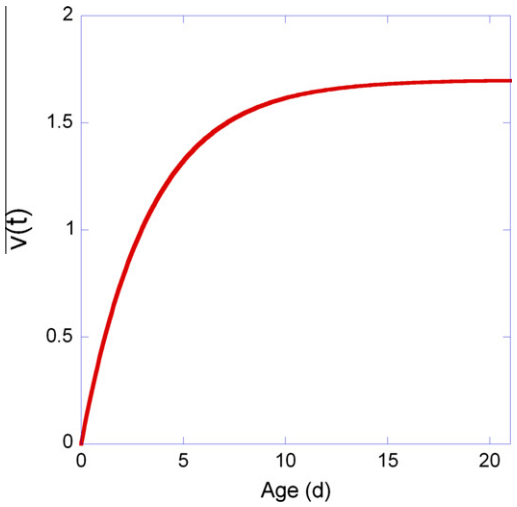

Fig. 2. Aging function for example problem. Since $v(t=1)=1$, the value obtained for E^0 will be that at an age of initial loading (displacement) of 1 d.

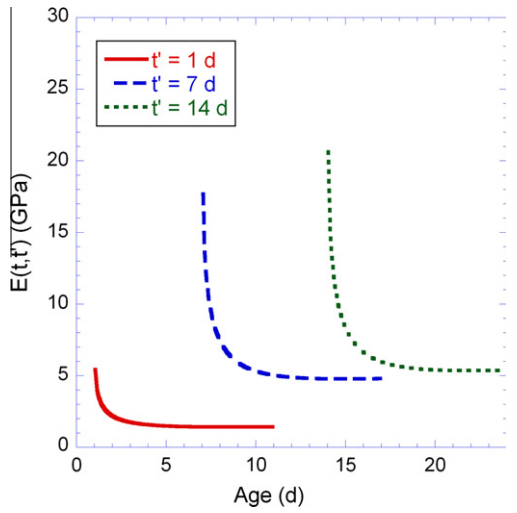

Fig. 3. Extracted $E^c(t,t')$ from ring tests with circumferential drying. t' reflects the age at which a constant displacement is first applied.

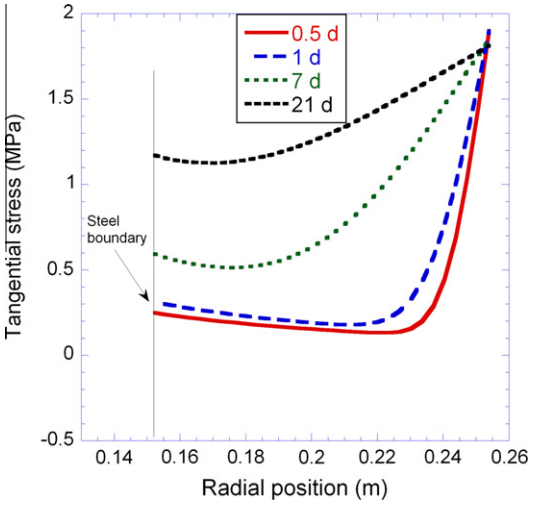

Fig. 4. $\sigma_\theta^c(r,t)$ of concrete subjected to various drying times assuming instantaneous elastic concrete properties.

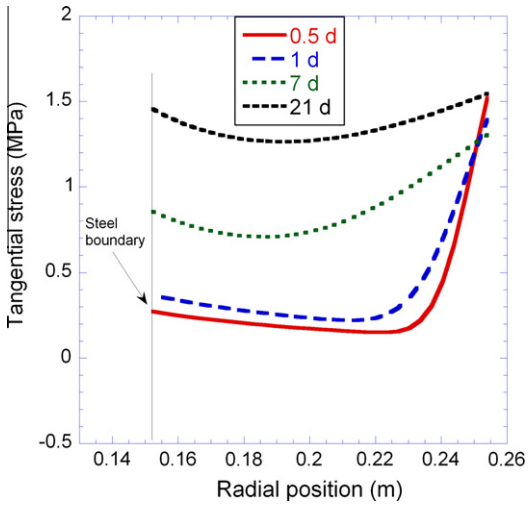

Fig. 5. $\sigma_\theta^c(r,t)$ of concrete subjected to various drying times assuming viscoelastic concrete properties.

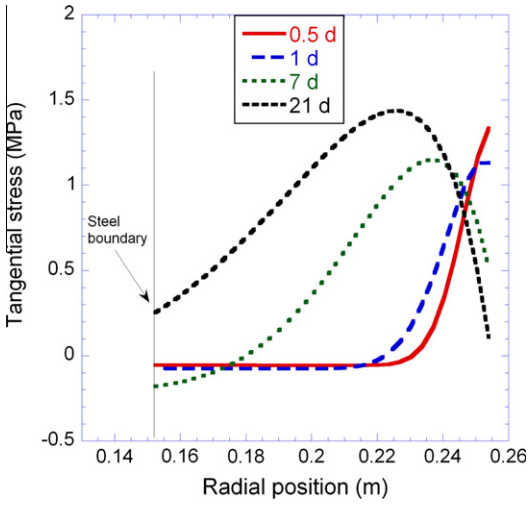

Fig. 6. $\sigma_\theta^c(r,t)$ of concrete subjected to various drying times assuming solidifying, viscoelastic concrete properties.

5.2. Determination of tangential stress profiles

The modified correspondence principle outlined in a previous section of this paper allows the determination of the tangential stress profile in the solidifying, viscoelastic concrete as a function of time. While others have predicted the stress profile in the restrained concrete ring test, earlier predictions have not accounted for the history effect inherent to viscoelastic materials nor the aging effect associated with solidification of concrete. Using the inputs from the previous section, $\sigma_\theta^c(r,t)$ in the concrete may be determined by (18), assuming instantaneous elastic properties only (i.e. viscoelasticity and solidification are ignored). In the case of viscoelastic concrete properties (neglecting solidification), $\sigma_\theta^c(r,t)$ may be determined by using (18) with the classic elastic–viscoelastic correspondence principle [22]. Finally, to determine $\sigma_\theta^c(r,t)$ for solidifying, viscoelastic concrete, the modified correspondence principle derived in this paper may be utilized to find

$$\overline{\sigma}_\theta^c(r,s)=\frac{(b-a)(a+b)\frac{E_s}{s}(c^2+r^2)D_1(s)}{2(b-c)(b+c)r^2}-\frac{2\kappa\overline{E}^g(s)((b^2+r^2)\overline{\underline{\varepsilon}}^f(s)-(b-c)(b+c)(D_2(s)-r^2\overline{\varepsilon}^f(r,s)))}{2(b-c)(b+c)r^2} \tag{35}$$

The parameter $D_2(s)$ is the Laplace transform of $\int_b^r r'\varepsilon^f(r',t)dr'$, which may be determined in the same fashion as $\overline{\varepsilon}^f(s)$, but with an upper limit of r rather than c on the integral in (33). Inversion of (35) results in $\sigma_\theta^c(r,t)$ for solidifying, viscoelastic concrete subject to the conditions and geometry outlined in the previous section.

Figs. 4–6 plot the elastic, viscoelastic, and solidifying viscoelastic $\sigma_\theta^c(r,t)$, respectively. In the elastic case, high tensile stress exists on the drying surface due to self restraint of the shrinkage gradient in the concrete. The tensile stress at the inner concrete surface is induced by the restraint of the inner steel ring. As expected, the average stress level gradually increases as drying progresses, although the peak stress on the surface is reached immediately upon the start of drying (since a fixed *RH* boundary condition is imposed). For the viscoelastic case, stress on the surface is reduced in comparison to the elastic case due to relaxation. However, because the same $\varepsilon_a(t)$ was used in the calculation of both the elastic and viscoelastic cases, the stress at the inner surface of the concrete ring is higher in the viscoelastic case than the elastic in order to create the same overall balancing interfacial pressure between the inner and outer rings necessary to satisfy equilibrium. The $\sigma_\theta^c(r,t)$ for the solidifying viscoelastic case is quite different than the elastic or viscoelastic cases. The drying surface stress still peaks immediately after exposure to drying conditions, but the solidification of new stress-free material after this initial application of shrinkage at the surface means that the stress gradually decays on the surface. The peak tensile stress migrates inward from the drying surface as drying progresses. Additionally, the stress at the interface with the restraining ring is much lower in the solidifying case. Overall peak tensile stresses are similar in the viscoelastic and the solidifying viscoelastic case, although they occur at different locations. It should be noted that the stress at the steel ring interface at the age of 21 d is probably under predicted for each case; this is due to the early drying limitation on the approximate functions used in the derivation. At an age of 21 d, the average internal *RH* in the concrete for this example problem has dropped below 75%, or below halfway between $RH_{initial}$ and RH_{bound}.

The implications of the differences between the predicted stress distributions considering elastic, viscoelastic, and solidifying viscoelastic concrete are significant. The solidifying viscoelastic case is expected to be the most realistic, although in reality, solidification effects are not likely to be as severe as indicated by the predictions in this paper since hydration rate decays rapidly with *RH* [26]. Neglecting solidification and viscoelastic effects may lead to inaccurate stress profiles that limit the utilization of the restrained ring test to assess the fracture of specific concrete mixtures.

6. Summary

Closed-form analytical solutions have been derived that allow the extraction of the viscoelastic Young's modulus of solidifying concrete from restrained concrete ring experiments. In addition, approximate solutions have been presented for predicting the internal *RH*, drying shrinkage, and tangential stress profiles in a drying ring exposed to a constant ambient *RH*. The example presented in the previous section shows calculated profiles for typical test conditions and a representative material. Viscoelastic effects result in a reduction in the drying surface stress in the concrete ring, but an increase in the inner surface stress in comparison to the elastic case with the same measured restrained ring strain. The effect of solidification is to cause a gradual reduction with time in the drying surface stress, and a shift inward from the drying surface of the peak tensile stress. Additionally, solidification reduces the tangential stress in the inner core of the material versus either the viscoelastic or elastic cases with the same measured restrained ring strain. The predicted stress profiles indicate that neglection of viscoelasticity and solidification of the concrete in the restrained ring test leads to an over prediction of surface and interface stress in the concrete ring.

Acknowledgments

This work was supported by the Texas Engineering Experiment Station and the Texas Transportation Institute.

Appendix A

The constitutive equation for the stress history of a solidifying, linear viscoelastic material may be expressed by [21]

$$\sigma(t)=\int_0^t v(t')\frac{\partial(\varepsilon(t')-\varepsilon^f(t'))}{\partial t'}E^g(t-t')dt'. \tag{A.1}$$

If the aging function is expressed according to (4), then the constitutive equation becomes

$$\sigma(t)=\kappa\int_0^t\left(1-e^{-\lambda t'}\right)\frac{\partial\left(\varepsilon(t')-\varepsilon^f(t')\right)}{\partial t'}E^g(t-t')dt'. \tag{A.2}$$

Taking the Laplace transform of (A.2) and utilizing the complex shift theorem, the transformed stress is obtained as

$$\begin{aligned}\overline{\sigma}(s)&=\kappa\overline{E}^g(s)[s(\overline{\varepsilon}(s)-\overline{\varepsilon}^f(s))]\\&\quad-\kappa\overline{E}^g(s)\left[(s+\lambda)(\overline{\varepsilon}(s+\lambda)-\overline{\varepsilon}^f(s+\lambda))\right],\end{aligned} \tag{A.3}$$

which simplifies to (5).

Appendix B

The internal *RH* distribution in a radially drying (from outer face only) concrete ring exposed to a constant ambient *RH* may be determined (assuming Fickian transport and a quasilinear diffusion coefficient) according to:

$$\begin{aligned}&\frac{\partial RH(r,t)}{\partial t}=\frac{1}{r}D\left(\frac{\partial}{\partial r}\left(r\frac{\partial RH(r,t)}{\partial r}\right)\right),\\&RH(c,t)=RH_{bound},\\&\frac{\partial RH}{\partial t}(b,t)=0,\\&RH(r,0)=RH_{initial}.\end{aligned} \tag{B.1}$$

Eq. (B.1) may be readily solved in the Laplace transform domain. Transforming (B.1) results in

$$\begin{aligned}&s\overline{RH}(r,s)-RH_{initial}=\frac{1}{r}D\left(\frac{\partial}{\partial r}\left(r\frac{\partial\overline{RH}(r,s)}{\partial r}\right)\right),\\&\overline{RH}(c,s)=RH_{bound}/s,\\&\frac{\partial\overline{RH}(b,s)}{\partial t}=0,\\&RH(r,0)=RH_{initial}.\end{aligned} \tag{B.2}$$

The solution of (B.2) results in an expression for $\overline{RH}(r,s)$ consisting of modified Bessel functions of the first and second kind. Using common algorithms [27], the numerical inversion of expressions containing modified Bessel functions often result in significant error or instability. However, an early drying period approximation for $\overline{RH}(r,s)$ may be obtained using the initial value theorem of Laplace transforms; this theorem states that

$$f(0^+)=\lim_{t\to0^+}f(t)=\lim_{s\to\infty}s\overline{f}(s). \tag{B.3}$$

Therefore, early drying may be approximated by utilizing asymptotic approximations for Bessel functions as $s\to\infty$:

$$I(i,j) \underset{s\to\infty}{\rightarrow} \frac{e^{j}}{\sqrt{2\pi j}}\left(1+\frac{(1-2i)(1+2i)}{8j}\right)$$
$$K(i,j) \underset{s\to\infty}{\rightarrow} \frac{\sqrt{\pi}e^{-j}}{\sqrt{2j}}. \tag{B.4}$$

In (B.4), $I(i,j)$ and $K(i,j)$ are the modified Bessel functions of the first and second kind, respectively, of order i and argument j. Combining the solution to (B.2) with (B.4)

$$\overline{RH}(r,s) = \frac{e^{-A_2}}{\frac{sA_1(1+A_3)}{(-A_1)^{3/2}\sqrt{A_2}}+\frac{A_4}{\sqrt{A_1}\sqrt{-A_2}}}\left\{\begin{array}{c}\frac{A_4\left(\frac{e^{A_6(\Delta RH)}}{\sqrt{-A_6}}+\frac{e^{A_2 RH_{initial}}}{\sqrt{-A_2}}\right)}{\sqrt{A_1}}-\\ \frac{(1+A_5)e^{A_6(\Delta RH)}}{\sqrt{A_6}}+\frac{(1+A_3)e^{A_2 RH_{initial}}}{\sqrt{A_2}}\\ \hline \sqrt{-A_1}\end{array}\right\}, \tag{B.5}$$

where

$$A_1=\frac{b\sqrt{s}}{\sqrt{D}} \quad A_3=\frac{\sqrt{D}}{8c\sqrt{s}} \quad A_5=\frac{\sqrt{D}}{8r\sqrt{s}}$$
$$A_2=\frac{c\sqrt{s}}{\sqrt{D}} \quad A_4=1-\frac{3\sqrt{D}}{8b\sqrt{s}} \quad A_6=\frac{r\sqrt{s}}{\sqrt{D}}, \tag{B.6}$$

and $\Delta RH = (RH_{bound} - RH_{initial})$. The quality of the early drying approximation given by (B.5) is illustrated in Fig. 7. The approximate and exact drying profiles are shown at four different reduced, dimensionless times (t/τ), where τ is a relaxation time expressed as

$$\tau = \frac{(c-b)^2}{D}. \tag{B.7}$$

Thus, Fig. 7 illustrates the accuracy of (B.5) with respect to the exact solution with the effects of geometry and the diffusion coefficient minimized through normalization. At early drying times, the approximation is very good. However, at later times (once the average internal RH drops below about half way between $RH_{initial}$ and RH_{bound}), the approximate solution begins to deviate, particularly at the inner boundary of the concrete cylinder (the interface with the restraining cylinder). The reason for the accuracy of (B.5) at early drying and inaccuracy at later times is the fact that a limit theorem was used to obtain a simplified analytical solution (i.e. the solution is exact as $t \to 0$).

The parameter $\overline{RH}(r,s)$ may be determined by integrating (33) and using (B.5) as an input to obtain

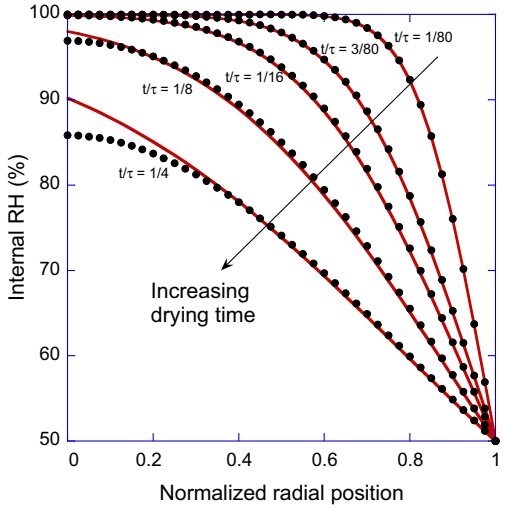

Fig. 7. Comparison of approximate internal RH gradient (lines) in concrete ring determined by inverting (B.5) with the exact solution (discrete points) at several reduced times (t/τ) after exposure to a constant $RH_{bound} = 50$.

$$\overline{RH}(r,s) = \frac{\sqrt{D}e^{-c\sqrt{s}/\sqrt{D}}(-bcs/D)^{3/2}}{2(3c+b)s^{3/2}} \times\left\{\frac{D^{3/2}\sqrt{-bcs/D}}{b^2c^2s^2}\times\left[-6c^{3/2}\left(\sqrt{6D}e^{B_1}-e^{B_3}\sqrt{Dr}\right)(\Delta RH)-B_4\right]+B_5\right\} \tag{B.8}$$

where

$$B_1=\frac{b\sqrt{s}}{\sqrt{D}}$$
$$B_2=\frac{c\sqrt{s}}{\sqrt{D}}$$
$$B_3=\frac{r\sqrt{s}}{\sqrt{D}}$$
$$B_4=-be^{B_2}(b-r)(b+r)RH_{initial}\sqrt{s}-3ce^{B_2}(b-r)(b+r)RH_{initial}\sqrt{s}$$
$$B_5=\frac{D^{7/4}\sqrt{\pi}(\Delta RH)\left(3\sqrt{D}-2b\sqrt{s}\right)\sqrt{-\frac{s}{D}}\left(Erfi\left(\frac{\sqrt{b}s^{1/4}}{D^{1/4}}\right)-Erfi\left(\frac{\sqrt{r}s^{1/4}}{D^{1/4}}\right)\right)}{b^{3/2}s^{9/4}}. \tag{B.9}$$

The term $Erfi(j)$ is the imaginary error function of argument j.

References

[1] Hossain AB, Pease B, Weiss J. Quantifying early-age stress development and cracking in low water-to-cement concrete: restrained-ring test with acoustic emission. Transport Res Rec 2003(1834):24–32.
[2] Hossain AB, Weiss J. Assessing residual stress development and stress relaxation in restrained concrete ring specimens. Cem Concr Compos 2004;26(5):531–40.
[3] Hossain AB, Weiss J. The role of specimen geometry and boundary conditions on stress development and cracking in the restrained ring test. Cem Concr Res 2006;36(1):189–99.
[4] Moon JH, Weiss J. Estimating residual stress in the restrained ring test under circumferential drying. Cem Concr Compos 2006;28(5):486–96.
[5] Moon J-H, Rajabipour F, Pease B, Weiss J. Quantifying the influence of specimen geometry on the results of the restrained ring test. J ASTM Int 2006;3(8):14–29.
[6] Schiessl P, Beckhaus K, Schachinger I, Rucker P. New results on early-age cracking risk of special concrete. Cem Concr Aggr 2004;26(2):139–47.
[7] See HT, Attiogbe EK, Miltenberger MA. Potential for restrained shrinkage cracking of concrete and mortar. Cem Concr Aggr 2004;26(2):123–30.
[8] Shah HR, Weiss J. Quantifying shrinkage cracking in fiber reinforced concrete using the ring test. Mater Struct 2006;39(293):887–99.
[9] Grasley ZC. Closed form solutions for uniaxial passive restraint experiments. ACI SP 2010;270:17–32.
[10] Carlson RW, Reading TJ. Model study of shrinkage cracking in concrete building walls. ACI Struct J 1988;85(4):395–404.
[11] Grzybowski M, Shah SP. Model to predict cracking in fibre reinforced concrete due to restrained shrinkage. Mag Concr Res 1989;41(148):125–35.
[12] Krauss PD, Rogalla EA, Sherman MR, McDonald DB, Osborn AEN, Pfeifer DW. Transverse cracking in newly constructed bridge decks. Washington, DC: National Council of Highway Research Projects; 1995.
[13] Krenchel H, Shah SP. Restrained shrinkage tests with pp-fiber reinforced concrete. ACI SP 1987;105:141–58.
[14] Whiting D, Detwiler R. Silica fume concrete for bridge decks. Washington, DC: National Cooperative Highway Research Program; 1988.
[15] Whiting DA, Detwiler RJ, Lagergren ES. Cracking tendency and drying shrinkage of silica fume concrete for bridge deck applications. ACI Mater J 2000;97(1):71–7.
[16] Lange DA, Roesler JR, D'Ambrosia MD, Grasley ZC, Lee CJ, Cowen DR. High performance concrete for transportation structures. Transportation engineering series. Urbana, IL: University of Illinois at Urbana-Champaign; 2003.
[17] See HT, Attiogbe EK, Miltenberger MA. Shrinkage cracking characteristics of concrete using ring specimens. ACI Mater J 2003;100(3):239–45.
[18] Hwang S-D, Khayat KH. Effect of mixture composition on restrained shrinkage cracking of self-consolidating concrete used in repair. ACI Mater J 2008;105(5):499–509.
[19] Grasley ZC, Lange DA. Constitutive modeling of the aging viscoelastic properties of portland cement paste. Mech Time Depend Mater 2007;11(3–4):175–98.
[20] Bažant Z. Viscoelasticity of solidifying porous material – concrete. J Eng Mech 1977;103(EM6):1049–67.

[21] Carol I, Bažant ZP. Viscoelasticity with aging caused by solidification of nonaging constituent. J Eng Mech 1993;119(11):2252–9.
[22] Read WT. Stress analysis for compressible viscoelastic materials. J Appl Phys 1950;21:671–4.
[23] Jaeger JC. On thermal stresses in circular cylinders. Philos Mag 1945;36:418–28.
[24] Grasley ZC, Lange DA. The viscoelastic response of cement paste to three-dimensional loading. Mech Time Depend Mater 2007;11(1):27–46.
[25] Bažant ZP, Baweja S. Justification and refinements of model b3 for concrete creep and shrinkage. 1. Statistics and sensitivity. Mater Struct/Mater Construct 1995;28(181):415–30.
[26] Jensen OM, Hansen PF, Lachowski EE, Glasser FP. Clinker mineral hydration at reduced relative humidities. Cem Concr Res 1999;29(9):1505–12.
[27] Graf U. Applied laplace transforms and z-transforms for scientists and engineers. Basel, Switzerland: Birkhauser Verlag; 2004.